DEVELOPMENTAL DYNAMICS 243:652–662, 2014
DOI: 10.1002/DVDY.24107

RESEARCH ARTICLE

Left Atrial Ligation Alters Intracardiac Flow Patterns and the Biomechanical Landscape in the Chick Embryo

William J. Kowalski,[1] Nikola C. Teslovich,[1] Prahlad G. Menon,[1] Joseph P. Tinney,[1,2] Bradley B. Keller,[1,2] and Kerem Pekkan[1]*

[1]Department of Biomedical Engineering, Carnegie Mellon University, Pittsburgh, Pennsylvania
[2]Department of Pediatrics, Cardiovascular Innovation Institute, University of Louisville, Louisville, Kentucky

Background: Hypoplastic left heart syndrome (HLHS) is a major human congenital heart defect that results in single ventricle physiology and high mortality. Clinical data indicate that intracardiac blood flow patterns during cardiac morphogenesis are a significant etiology. We used the left atrial ligation (LAL) model in the chick embryo to test the hypothesis that LAL immediately alters intracardiac flow streams and the biomechanical environment, *preceding* morphologic and structural defects observed in HLHS. **Results:** Using fluorescent dye injections, we found that intracardiac flow patterns from the right common cardinal vein, right vitelline vein, and left vitelline vein were altered immediately following LAL. Furthermore, we quantified a significant ventral shift of the right common cardinal and right vitelline vein flow streams. We developed an *in silico* model of LAL, which revealed that wall shear stress was reduced at the left atrioventricular canal and left side of the common ventricle. **Conclusions:** Our results demonstrate that intracardiac flow patterns change immediately following LAL, supporting the role of hemodynamics in the progression of HLHS. Sites of reduced WSS revealed by computational modeling are commonly affected in HLHS, suggesting that changes in the biomechanical environment may lead to abnormal growth and remodeling of left heart structures. *Developmental Dynamics 243:652–662, 2014*. © 2013 Wiley Periodicals, Inc.

Submitted 30 May 2013; First Decision 16 September 2013; Accepted 20 September 2013; Published online 19 December 2013

Introduction

Hypoplastic left heart syndrome (HLHS), is a rare but serious congenital heart defect, occurring in 1 of every 5,000 births (Go et al., 2013). The hallmarks of HLHS are an underdeveloped and nonfunctioning left ventricle and hypoplastic ascending and transverse aorta in association with stenosis or atresia of the mitral and/or aortic valves, and intra-uterine compensatory enlargement of right sided cardiac structures (Friedman et al., 1951; Noonan and Nadas, 1958). A genetic component for HLHS is supported by studies that examined heritability, which show that HLHS is linked to chromosomes 10q and 6q and genetically related to bicuspid aortic valve (Hinton et al., 2007, 2009), although the strength of this relationship is unknown (McBride et al., 2009). The genetic basis of HLHS is still largely undetermined and no transgenic animal models have recapitulated the human HLHS phenotype (Sedmera et al., 2005). Clinical innovations and scientific research has significantly improved the outlook for infants born with HLHS from a fatality rate of over 95% in 1980 to our current projections that 70% of infants born with HLHS are expected to survive to adulthood (Feinstein et al., 2012). These advances in diagnostic and treatment strategies are remarkable; however, the pathogenesis of HLHS during embryonic and fetal life remains poorly understood. Fetal interventions have become available with the goal of positively impacting fetal and post-natal cardiac growth and remodeling.

For most of its history, HLHS has been classified as a "flow defect," attributed to altered hemodynamic loading of the left heart structures, and fetal echocardiography has demonstrated that blood flow patterns have an important role in the development of HLHS (Grossfeld et al., 2009). An abnormally small or absent foramen ovale may be one key component, reducing flow to the left heart and impairing normal growth of left heart structures (Chin et al., 1990; Feit et al., 1991; Rychik et al., 1999), and one study has shown a correlation between diameter of the foramen ovale and relative right heart and/or left heart flow (Atkins et al., 1982). Obstructed inflow or outflow of the left ventricle due to valvular defects is more likely, however, as there is a strong correlation between the diameter of the left atrioventricular junction and left ventricle or aortic root (Sedmera et al., 2005). While the initial insult causing HLHS, genetic or structural, is unknown, the resulting hemodynamic alterations are significant and progressive. A typical diagnostic scenario in the clinic is detection of normal left heart dimensions with reduced function at mid-gestation, which is later followed by progressive involution of the left ventricle in the third trimester of pregnancy (McElhinney et al., 2010). One unifying hypothesis is that altered intracardiac flow patterns (ICFP) and altered mechanical loading

Additional Supporting Information may be found in the online version of this article.
Grant sponsor: NSF; Grant number: CAREER Award 0954465; Grant sponsor: Kosair Charities Pediatric Heart Research Program.
*Correspondence to: Kerem Pekkan, Biomedical and Mechanical Engineering, Carnegie Mellon University, 700 Technology Drive, Pittsburgh, PA 15219. E-mail: kpekkan@andrew.cmu.edu

Article is online at: http://onlinelibrary.wiley.com/doi/10.1002/dvdy.24107/abstract

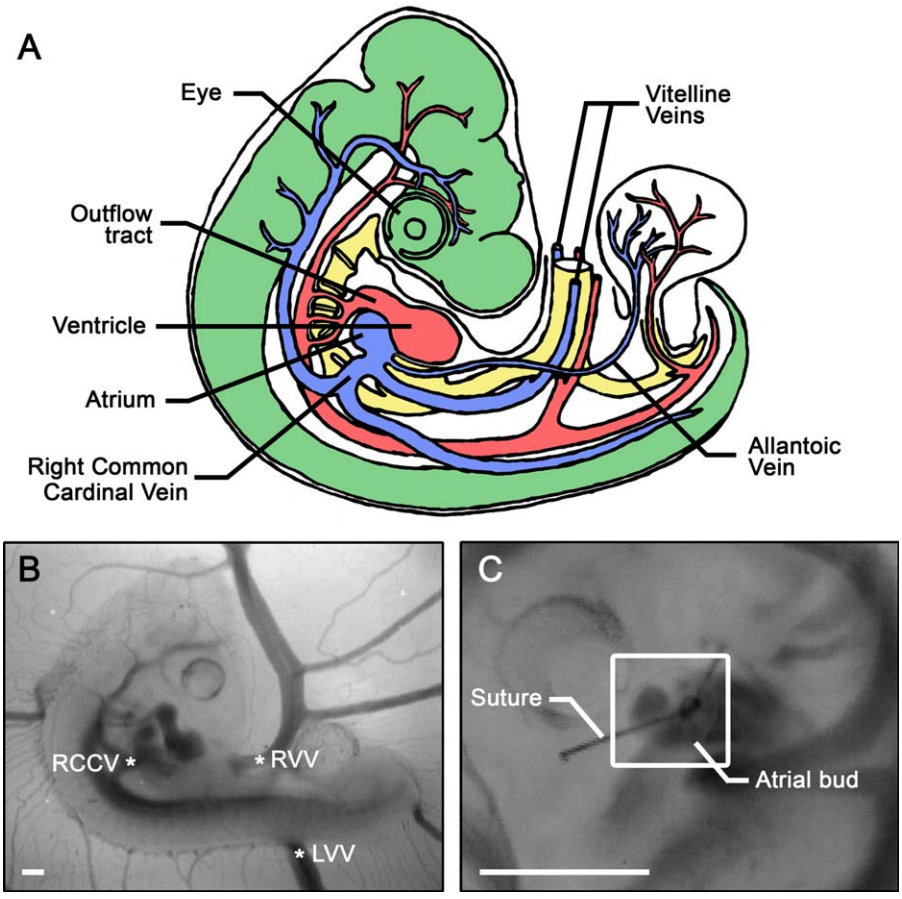

Fig. 1. The stage 21 chick embryo experimental model. **A:** Schematic of a stage 21 chick embryo, right lateral perspective. Vascular structures are labeled, where blue represents venous vessels and red arterial vessels. Green and yellow show neuronal and digestive structures, respectively. **B:** Stereomicroscope image of a normal stage 21 embryo, viewed from the right lateral perspective. Venous injection sites used in this study are labeled. The right common cardinal vein (RCCV) is the confluence of the right anterior and posterior cardinal veins, which drain blood from the embryo proper. The left and right vitelline veins (LVV, RVV) return blood from the extraembryonic vitelline bed. **C:** Stereomicroscope image of an LAL embryo, viewed from the left lateral perspective. The primitive left atrium is tied off with a 10-0 nylon suture. All scale bars = 500 μm.

conditions result in left ventricular hypoplasia due to the lack of sufficient mechanical loading to stimulate cardiac growth and remodeling. This hypothesis has been applied as a rationale for fetal interventions, in which fetal balloon aortic valvuloplasty is performed to restore normal antegrade aortic flow and left ventricular loading conditions (McElhinney et al., 2010).

A large number of transgenic animal models have revealed key roles for signaling pathways and transcription factors in many of the events required for normal cardiovascular development, including outflow tract septation (Franz, 1989; Tallquist and Soriano, 2003), valve morphogenesis and remodeling (de la Pompa et al., 1998; Ranger et al., 1998; Dunker and Krieglstein, 2002; Hurlstone et al., 2003), and myocardial contraction (Bartman et al., 2004). However, embryonic models that alter the mechanical environment in the setting of a normal genotype are limited. These studies are usually performed in avian embryos, mainly represented by vitelline vein ligation (Rychter and Lemez, 1965; Hogers et al., 1997), conotruncal banding (Clark et al., 1989), and left atrial ligation (Rychter and Lemez, 1958; Sedmera et al., 1999). Acquiring reliable, spatially resolved velocity measurements in the embryonic heart remains challenging, and many studies lack a quantitative analysis of the biomechanical environment after these perturbations. Newborn and juvenile models of univentricular circulation have been developed in sheep to monitor cardiac function after repair of HLHS, although their long-term success and application is limited (Rodefeld et al., 2003; Myers et al., 2006). Further research using these existing mechanical models, and the development of novel models, is necessary to understand the role of hemodynamics and optimize fetal intervention strategies (Pekkan and Keller, 2013).

The chick embryo has been widely used as a model for vertebrate cardiovascular development (Pexieder, 1986; Martinsen, 2005). Left atrial ligation (LAL) in the chick embryo remains the only long-term prenatal animal model of HLHS (Rychter, 1962). In the LAL model, tying off the presumptive left atrium as a recoverable procedure disrupts inflow to the left side of the embryonic ventricle. Measured as early as one hour after ligation, cardiac output is transiently reduced, returning to normal levels by 32 hours post-LAL, while downstream cardiac pressures remain normal throughout (Lucitti et al., 2005). Signs of remodeling of the ventricular myocardium can be observed 2 days after ligation, including decreased myocardial volume, accelerated trabecular compaction, and delayed changes in transmural myofiber angle (Sedmera et al., 1999; Tobita et al., 2005). Circumferential and longitudinal strain increases in both ventricles after LAL, while the onset of preferential circumferential strain patterns in

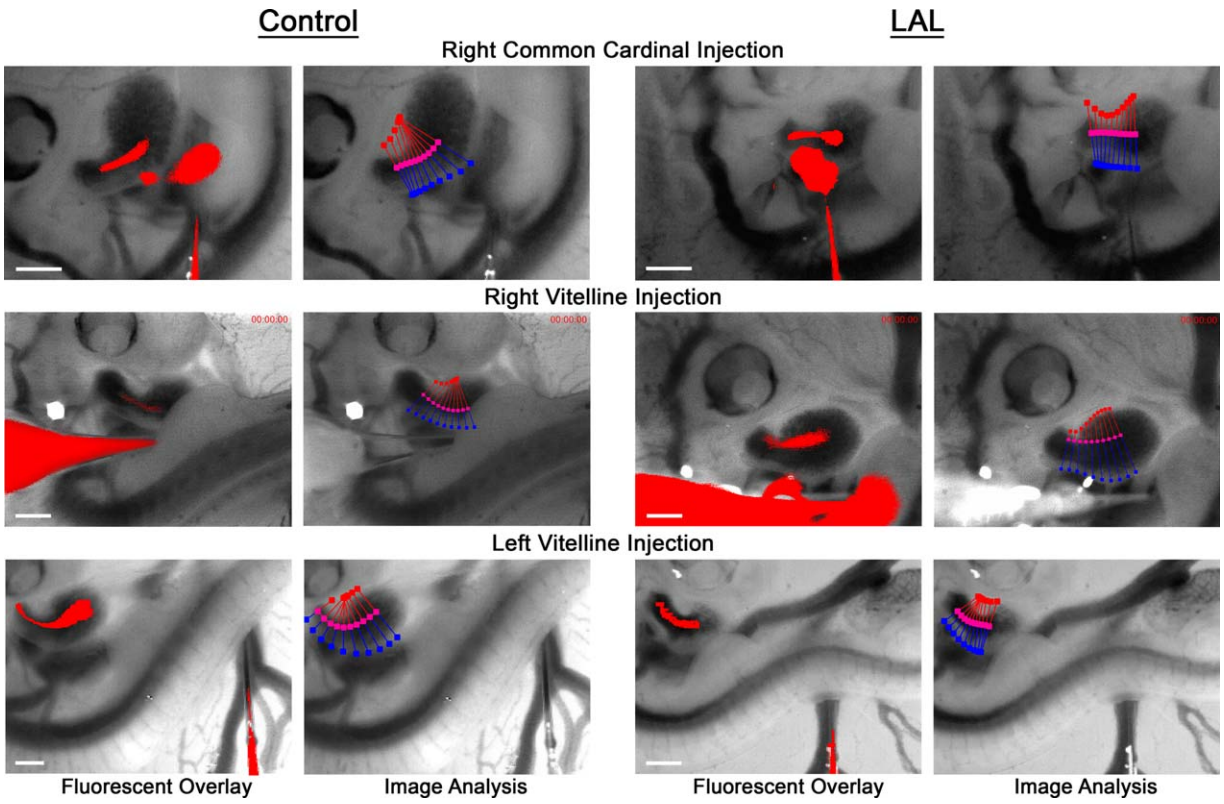

Fig. 2. Representative images from the experimental fluorescent dye injections. Control embryos are on the left and LAL embryos are on the right. For each injection site, the overlay of the fluorescent and brightfield image is shown alongside the output of the image analysis to measure the distance between the flow stream (pink) and the ventral (red lines) and dorsal (blue lines) walls of the heart. All scale bars = 250 μm.

the right ventricle are accelerated and the preferential longitudinal strain patterns in the left ventricle are abolished (Tobita and Keller, 2000). Cellular changes after LAL include reduced proliferation in the left ventricular compact layer and trabeculae, decreased expression of FGF-2 and PDGF-B throughout the heart, and an increased number of apopototic cells in the right atrioventricular cushions (Sedmera et al., 2002), as well as increased microtubule density in the left ventricular compact layer (Schroder et al., 2002). Despite the limited number of studies focusing on vascular development compared with the ventricle, downstream vessels are also affected in LAL; flow distribution within the aortic arches is disrupted, and defects including aortic arch hypoplasia and interrupted aortic arch are observed as early as 32 hr after ligation (Hu et al., 2009).

These previous studies clearly demonstrate the morphologic, structural remodeling, and cellular consequences of LAL. However, to date there has not been a *quantitative* analysis of changes in ICFP that occur following LAL. While hemodynamic anomalies such as reduced left ventricular filling and mitral, tricuspid, and aortic valve regurgitation have been recorded, these were observed 4 days post-LAL (deAlmeida et al., 2007). The immediate effects of LAL (<1 hr after ligation) on flow patterns are therefore unknown. Furthermore, quantitative analysis of hemodynamic loading after LAL has not been performed. In this study, we test the hypothesis that ICFP are altered immediately following LAL. Validation of this hypothesis would demonstrate that changes in ICFP precede changes in ventricular morphology and structure, supporting the idea that flow patterns are a primary factor in the production of the HLHS phenotype after LAL. We applied a quantitative analysis of fluorescent dye microinjections to map the location of the intracardiac flow stream within the ventricle and outflow tract. We further developed a computational fluid dynamics (CFD) model of the normal and LAL heart loop to estimate changes in wall shear stress (WSS) that may occur due to the occlusion of the left atrium. Our results show that the position of the intracardiac flow stream is shifted significantly in two of the three venous injection sites and that WSS is reduced at the left atrioventricular canal and left ventricle. Thus, LAL immediately re-routes flow through the heart, likely causing reduced biomechanical loading and growth of left heart structures and leading to impaired remodeling and eventual HLHS.

Results

Intracardiac Flow Streams in Normal and LAL Embryos

We performed LAL at Hamburger-Hamilton stage 21 (Hamburger and Hamilton, 1951; Al Naieb et al., 2013). At stage 21, cardiac looping is largely complete, with only minor migration and rotation of the outflow tract progressing through stage 24 (Manner, 2000). The left and right atrial cavities have formed and ventricular trabeculation is present, although neither septum has fully formed (Martinsen, 2005). The dorsal and ventral atrioventricular canal cushions have started to form (De la Cruz et al., 1983), and four of the five primary outflow tract cushions are present (Qayyum et al., 2001). Blood enters the common atrium through several venous sites including the vitelline veins (VV), which drain the vitelline bed, the right and left common cardinal veins

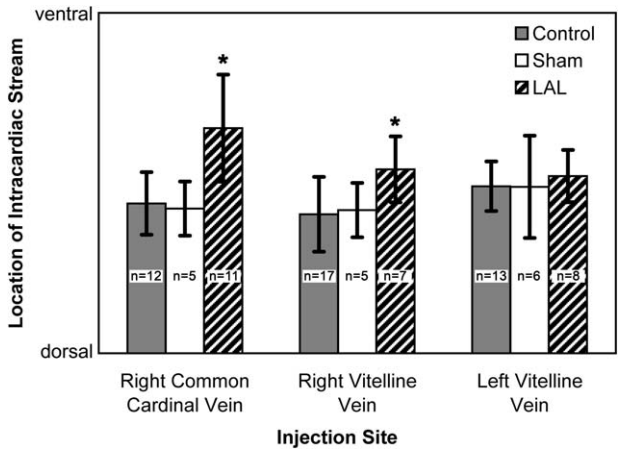

Fig. 3. Results of the intracardiac stream measurements. The average location of the stream in control, sham, and LAL embryos is shown. Error bars represent the standard deviation. Numbers within each bar indicate the sample size. * Indicates a statistically significant ($P < 0.05$) difference vs. the control group.

(CCV), which return blood from the embryo proper, and the allantoic veins, which drain the allantois (Fig. 1). Blood is ejected through the common outflow tract and symmetric, bilaterally paired aortic arches. Most often three aortic arch pairs are present at stage 21, although a variety of patterns have been documented associated with flow and vessel caliber mismatch (Kowalski et al., 2013). The stage 21 embryonic heart rate is 155 beats per minute and cardiac output is 1.28 mm^3/s (Hu and Clark, 1989).

To visualize flow streams, we injected embryos with fluorescent dye at three different venous sites: (1) the right CCV (RCCV), (2) the right VV (RVV), and (3) the left VV (LVV) (Fig. 1). Each embryo was injected once; sham and LAL embryos were injected after a reincubation period lasting less than 1 hr. We computed a normalized intracardiac stream position from the recorded injections. Blood flow was laminar in all embryos. The heart continued to beat at a constant rate for a minimum of one minute after dye injection, allowing us to record multiple cardiac cycles. Low Reynolds number flow in the embryonic ventricle does not allow flow stream mixing. After removing the needle, blood hemorrhaged and the heart beat ceased rapidly afterward. Our fluorescent dye injections and image analysis allowed us to quantitatively compute the position of the intracardiac flow stream within the common ventricle and outflow tract. Results of our experimental dye injections are summarized in Figures 2 and 3, and fluorescent overlay movies of representative injections are provided in the Supplemental Material, which are available online. Our normalized stream position represents the distance from the dorsal wall of the embryonic heart, where 0 is exactly the dorsal wall and 1 is exactly the ventral wall. For control embryos, we found that dye injected at the RCCV took a slightly dorsal route, with an average stream location of 0.44 ± 0.09 ($n = 12$). The stream from the RVV was the most dorsal, with a position of 0.41 ± 0.11 ($n = 17$). The location of the LVV stream was 0.49 ± 0.07 ($n = 13$), directly through the midline of the heart. Sham embryos displayed similar ICFP, with no significant differences vs. the control group.

The response of LAL embryos to insertion of the micro needle was similar to control embryos with no observable effect on hemodynamics or heart rate. For LAL embryos, our quantitative analysis revealed that the RCCV stream changed significantly ($P < 0.05$), now taking a ventral course through the ventricle and outflow tract, with an average location of 0.66 ± 0.16 ($n = 11$). The RVV stream also shifted toward the ventral side of the heart ($P < 0.05$), positioned at 0.54 ± 0.10 ($n = 7$). The intracardiac path of the LVV remained similar at 0.52 ± 0.08 ($n = 8$, $P > 0.05$). In the LAL embryos, the RCCV and RVV streams were ventral to the LVV stream, the reverse of the control ICFP. Of interest, all flow patterns shifted ventrally, although only the RCCV and RVV were significantly changed compared with the controls. We also observed some retrograde flow in the LAL embryos, where dye injected at the RVV and LVV would flow into the cardinal veins. These results demonstrate that LAL significantly alters ICFP in the embryo, and that this change occurs immediately following the intervention.

In Silico LAL Model

We performed three-dimensional (3D) CFD simulations of steady flow through control and LAL models of the stage 21 heart loop. Both models were created in the computer using our in-house surgical planning suite (Pekkan et al., 2008; Dur et al., 2011). Blood flow was modeled using our in-house immersed boundary cardiovascular flow solver, which has previously been validated for models of the stage 11, 13, and 18 heart loop, comparing accurately with the commercial second-order unstructured grid flow solver Fluent (version 6.3.26, ANSYS Inc., Canonsburg, PA) and experimental microfluidic models of the embryonic heart tube (Supp. Fig. S1; Pekkan et al., 2009). Mean total cardiac output was 1.28 mm^3/s, equivalent to stage 21 Doppler flow measurements (Yoshigi et al., 2000), and rigid, no-slip walls were assumed for simplicity, simulating mean quasi-steady flow conditions in the heart. We computed color-coded flow streamlines originating from the right and left vitelline veins to observe ICFP in our CFD models (Fig. 4). There were some subtle differences, including an overall ventral shift of the flow streams in the LAL model (Fig. 4). This movement of ICFP toward the ventral margin of the heart is similar to our experimental observation. Flow from the RVV seemed to follow the inner curvature of the heart more tightly in the LAL model as well. However, the variation between the control and LAL CFD models is far less pronounced than the experimental results, and we did not observe the reversal of RVV and LVV stream positions (Fig. 4), prompting future improvements in computational model. We computed the velocity profile at the outflow tract and found that it was slightly more skewed in the ventral and left directions in the LAL vs. control model.

To examine changes in biomechanical loading that occur due to removal of the left atrium, we calculated WSS from our CFD results (Fig. 5). The maximum WSS levels in the heart were 3.5 Pa, found at the CCV and VV inlets and the ventral side of the outflow tract outlet, consistent with WSS values derived from particle image velocimetry in similar stage chick embryos (Poelma et al., 2010). Compared with the control model, WSS in the LAL model was reduced at the left side of the atrioventricular canal and left side of the common ventricle (Fig. 5). WSS was also slightly increased at the ventral surface of the distal outflow tract. These simplified, static CFD models show that redistribution of the left atrial volume is sufficient to alter ICFP and WSS loading, while the disparity with the experimental results supports the

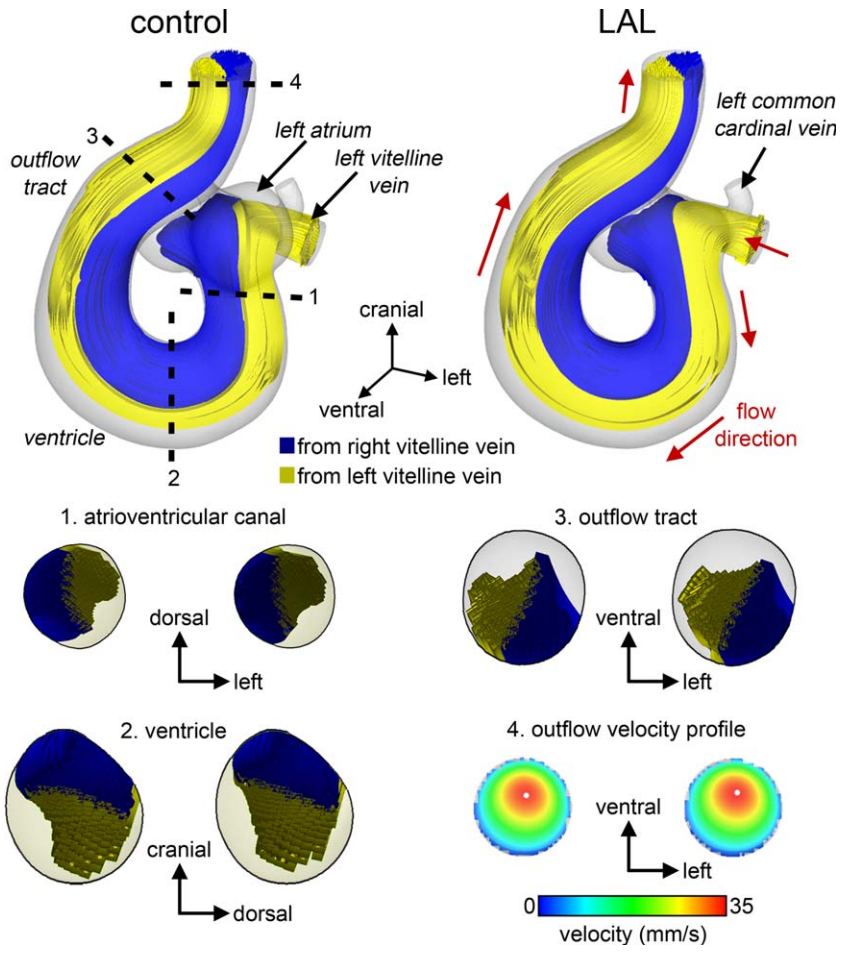

Fig. 4. Intracardiac flow patterns in CFD models of control and in silico LAL embryonic cardiac geometries. The control model is on the left and the LAL model is on the right. In the upper figures, color coded streamlines are shown, with blue representing flow emanating from the RVV and yellow depicting flow from the LVV. Red arrows give the forward flow direction. The bottom panels show cross-sections at each of the sites labeled in the control flow stream figure. Control cross-sections are on the left and LAL on the right. The cross-sections reveal a slight overall ventral shift of flow paths in the LAL model. The velocity profile at the outflow tract is shown for cross-section 4, where a slight ventral shift of the peak flow location is observed in the LAL model.

additional roles of the endocardial cushions and dynamic ventricular suction during relaxation in determining ICFP.

Discussion

Qualitative description of normal ICFP in the chick embryo has been taken up by several authors, giving rise to some contradictions (Bremer, 1932; Rychter and Lemez, 1965; Jaffee, 1967; Yoshida et al., 1983; Hogers et al., 1995). Early studies attempted to follow red blood cells as they coursed through the heart, and led to the widely perceived notion that two separate streams spiraled around each other through the outflow tract (Bremer, 1932; Jaffee, 1967). The presence of these streams was thought to shape the spiral aortopulmonary septum, with anomalous spiraling proposed as a major cause of septation defects (Jaffee, 1965). This notion was challenged when researchers began injecting dyes or India ink and did not observe spiraling outflow streams (Yoshida et al., 1983; Hogers et al., 1995). In their comprehensive study of chick embryos between stages 14 and 22, Yoshida et al. observed two types of intracardiac streams which depended on both injection site and developmental age (Yoshida et al., 1983). These streams did not spiral around one another, but rather followed a dorsal or ventral path through the ventricle and outflow tract. These patterns were later confirmed by Hogers et al. using India ink injections of embryos between stages 12 and 17 (Hogers et al., 1995). Their study revealed distinct ICFP for blood emanating from different yolk sac regions, further demonstrating the significance of venous return sites and the presence of multiple simultaneous ICFP. Our ICFP observed in control stage 21 embryos matched those of Yoshida et al. (1983), with blood from the RVV taking a more dorsal path compared with blood from the LVV. No study has examined either CCV. In no cases of these embryonic did we observe evidence of spiraling streams through the outflow tract. The work of Yoshida et al. also suggested that blood from the RVV and LVV perfused only the ipsilateral aortic arches at stage 21 (Yoshida et al., 1983). This pattern was contradicted by other studies, which showed that the distribution through the aortic arches was not a simple left and right current (Rychter and Lemez, 1965; Hogers et al., 1995; Hu et al., 2009). While we did not examine ICFP beyond the outflow tract in this study, our previous investigations dedicated to the aortic arches

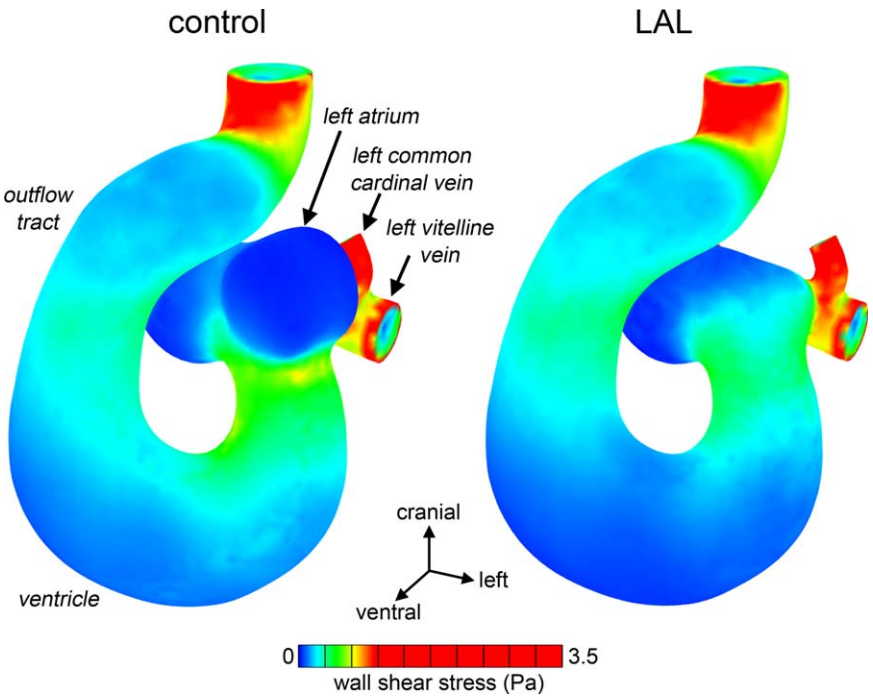

Fig. 5. WSS computed from CFD models of control and *in silico* LAL embryonic cardiac geometries. The control model is on the left and the LAL model is on the right. Reduced WSS can be seen at the left side of the atrioventricular canal and left region of the common ventricle. Increased WSS is located at the ventral side of the distal outflow tract. To display a broader range of WSS, a peak WSS of 1.0 Pa is shown.

corresponds with a complex perfusion pattern (Wang et al., 2009; Kowalski et al., 2013).

Yoshida et al. observed nearly the exact reverse ICFP in embryos stage 17–18: blood from the RVV took a more ventral route compared with blood from the LVV, and the two streams perfused the contralateral aortic arches (Yoshida et al., 1983). These patterns transitioned at around stage 19, and the authors attributed the dramatic reversal to the changes in the vitelline venous system. Our data show that in LAL stage 21 embryos, blood from the RVV courses more ventrally compared with blood from the LVV, similar to the stage 17–18 patterns described by Yoshida et al. (Fig. 2). It may be that obstruction of the left atrium prevents the change in RVV and LVV patterns or returns ICFP to their earlier state. Before stage 18, the atrial cavities are small and hardly distinguishable from the heart tube. Between stages 18 and 21, however, the atria significantly increase in size, particularly the left atrium, which becomes larger than the right (Manner, 2000; Kim et al., 2011; van den Berg and Moorman, 2011; Yalcin et al., 2011). This expansion of atrial volume and the atrial contribution to ventricular filling may relate to the change in ICFP, which occurs during the same interval. As the expansion of the left atrium is more pronounced than the right, its ligation may return the cardiac geometry to resemble stage 17, causing ICFP to revert. Ventricular trabeculation may also have a role in the changing flow patterns at stage 19. Beginning at stage 16/17, trabeculation progresses rapidly during this period, and is largely responsible for increases in myocardial mass (Sedmera et al., 2000). Another key morphologic event occurring during the period between stages 17 and 25 involves substantial growth and remodeling of the endocardial cushions lining the atrioventricular canal and outflow tract, brought on by the invasion of cells that begin to undergo epithelial to mesenchymal transformations at stage 17 (Noden, 1991; Butcher et al., 2007). LAL may interfere with these events by preventing growth of the left atrium, limiting the expansion of the atrioventricular canal, or displacing the endocardial cushions.

Our numerical control vs. LAL CFD models confirmed the variation in the location of the flow streams originating from the RVV and LVV, but these are less pronounced that the in vivo injections (Fig. 4). A major difference is that we do not see the dramatic ventral shift of the RVV flow stream after LAL. Presently, our CFD model did not incorporate the endocardial cushions or ventricular trabeculae and applied rigid, no-slip walls and steady, unidirectional flow, ignoring the AV synchronous contractions and pulsatile flow environment. Furthermore, the external boundary conditions specified at the vessel inlet and outlets, as well as the neglected wall movement, may suppress the *in vivo* observed internal flow differences. These limitations influence the numerical model of ICFP and mask key elements of the biomechanical environment such as oscillatory WSS. Effects of flow pulsatility may be less important, illustrated in our previous pulsatile CFD models of the stage 18 heart loop, which revealed that Womersely numbers were low (0.44), suggesting that the effects of pulsatile flow are small (Pekkan et al., 2009). The assumptions described above were necessary to reduce computational time and produce a solvable model. Differences between the computational model and experiment may indicate that those aspects absent from the model, such as cardiac contractions, endocardial cushions, and ventricular trabeculae, are vital to establishing ICFP. Even without these features, however, our models show that simply removing the left atrium can alter the course of blood and WSS levels in the heart realistically. In particular, WSS was reduced at the left side of the common ventricle and left wall of the atrioventricular canal and slightly increased on the ventral

surface of the outflow tract (Fig. 5). WSS differed by 0.5 Pa at these sites, which is above the known threshold to initiate an endothelial response (Egorova et al., 2011). These areas are commonly affected in HLHS, suggesting that LAL may redirect flow to unload the presumptive left ventricle and its inflow. The velocity profile change in the in silico LAL model may indicate a reason for altered aortic arch perfusion and defects in LAL embryos (Hu et al., 2009). However, our recent simulations of aortic arch flow using various velocity profile shapes at the outflow tract do not show significant changes in flow distribution or WSS, again demonstrating the importance of the dynamic contractions (Kowalski et al., 2013).

Morphogenesis of the veno-atrial region is ongoing at stage 21, and the veno-atrial connections may differ between embryos (Manner and Merkel, 2007; van den Berg and Moorman, 2011). Our model geometry includes proximal separation of the right and left vitelline veins, a centrally located venous sinus, and symmetric cardinal veins, all of which are characteristic of the early state of veno-atrial morphogenesis (Fig. 4). By stage 24, however, the proximal vitelline veins have fused, the sinus connection is limited to the right atrium, and the left cardinal vein is elongated. As this transformation likely influences ICFP, we modified our model geometry to correspond with this later state venous anatomy and repeated our control and LAL flow models (Supp. Fig. S2). As with our original geometry, flow patterns in the LAL model were not substantially different from the control. This later state model, therefore, reinforces our previous reasoning that those features not incorporated, i.e. cardiac contractions, endocardial cushions, and ventricular trabeculae, have a role in directing intracardiac blood flow. We did find, however, that the outflow velocity profile was more skewed in the ventral direction after changing the venous morphology (Fig. 4 and Supp. Fig. S2). These two models suggest that morphogenesis of the sinuatrial region can influence ICFP and may provide an explanation for the changes in flow patterns that occur in normal embryos from stages 18 to 24 (Yoshida et al., 1983).

Static CFD models of flow in the human embryonic heart show the presence of multiple simultaneous intracardiac streams, with patterns similar to those observed in the chick embryo, demonstrating the relevance of these animal models to human development (DeGroff et al., 2003). While success has been made in reconstructing static embryonic cardiac geometries from polymeric casting (Wang et al., 2009; Yalcin et al., 2011), there is no existing model of the dynamic embryonic heart. Recent techniques have simulated blood flow in the contractile outflow tract (Liu et al., 2011), although this work is in nascent stages and has yet to incorporate the upstream heart and downstream vessels. Validation of such models will require information of 3D velocity profile shapes in vivo. We have recently explored a combined particle image velocimetry and optical coherence tomography technique to acquire velocity measurements noninvasively, which can be applied to future studies (Chen et al., 2012).

Numerous studies using chick (Gessner, 1966; Hogers et al., 1997, 1999; Reckova et al., 2003; Lucitti et al., 2006) and zebrafish (Hove et al., 2003; Chen et al., 2011; Corti et al., 2011) embryos support the role of hemodynamics in modifying cardiovascular growth, morphogenesis, and remodeling. It is well established that WSS is a key environmental factor affecting cardiovascular development in the embryo and adaptation in the adult (Rodbard, 1975; Langille and O'Donnell, 1986; Girerd et al., 1996; Bayer et al., 1999; Culver and Dickinson, 2010). Using an RVV ligation model, Hogers et al. found that ICFP emanating from four yolk sac regions followed altered routes through the heart and outflow tract, leading to defects such as small to large ventricular septal defects, bicuspid aortic valve, and aortic arch anomalies (Hogers et al., 1997). This ligation model was further shown to cause spatial and temporal changes in the transcriptional profile of genes encoding Krüppel-like factor (increased), endothelin-1 (decreased), and endothelial nitric oxide synthase (decreased), suggesting increased WSS (Groenendijk et al., 2005). The increased WSS in the outflow tract was also associated with higher Tgfβ/Alk5 signaling, a phenomenon which was sensitive to the level of WSS (Egorova et al., 2011). This mechanosensitivity of endocardial cells, coupled with the changed ICFP after LAL, likely results in abnormal morphogenesis and remodeling of the atrioventricular and outflow tract cushions, leading to valve defects normally present in HLHS. Although our technique does not capture total flow through the atrioventricular canal, the quantitative measurements through the outflow tract show a significant ventral shift of the RVV and RCCV streams (Fig. 3). In the RVV ligation model of Hogers et al., flow streams from two of the four yolk sac regions saw a similar dorsal to ventral shift (Hogers et al., 1997). It is interesting that the outlet of the left ventricle is dorsal to that of the right ventricle in the mature chick. The lack of a dominant dorsal stream after LAL may cause reduced WSS on the dorsal cushions present at stage 21, impairing the formation of the left ventricle outflow tract and aortic valve.

Our experiments support the hypothesis that LAL immediately alters ICFP in the chick embryo. We quantitatively showed a significant ventral shift in both the RVV and RCCV flow streams. While the LVV flow stream did not change significantly, the LVV and RVV streams switched relative positions in LAL compared with control hearts, resembling earlier stage 18 patterns (Yoshida et al., 1983). Our static CFD model of the embryonic heart loop further revealed that removing the left atrium volume was sufficient to alter WSS at critical locations within the left heart. These results suggest that changes in ICFP following LAL precede structural defects such as bicuspid aortic valve and the characteristic undersized left ventricle. The concordance between control and sham embryos suggests that the manipulations required to perform LAL do not cause a change in flow patterns. However, the ligation itself may cause structural damage to the heart, which can affect its further development. While we take great care and reject any embryos that show bleeding after LAL, we cannot rule out this trauma as a cause for HLHS defects. Therefore, we conclude that the change in ICFP occurs early in development of HLHS after LAL, but may not be the only or initial insult.

Experimental Procedures

Experimental Measurement of Intracardiac Stream Position

Embryo preparation and injection

Fertile white Leghorn chicken eggs were incubated blunt end up in a forced draft incubator at 37°C and 50% humidity for 84 hr to Hamburger-Hamilton stage 21 (Hamburger and Hamilton, 1951; Al Naieb et al., 2013). To access the developing embryo, we gently cracked the eggshell above the air sac and peeled back the shell and membrane to form a 1-cm^2 window. We then removed

the overlying extraembryonic membrane using microforceps (Dumont M5, WPI, Sarasota, FL). Limb size, spinal curvature, and the presence of body tissues were used to stage embryos, and any that were dysmorphic, such as lacking retina, displaying axial twisting, or left side up were excluded. To perform LAL, we positioned embryos *in ovo* under a stereomicroscope (Leica M165F, Leica Microsystems GmbH, Germany), dissected the amniotic membrane, and flipped the embryo to reveal the presumptive left atrium. We used microforceps to make a slit-like opening in the thoracic wall above the atrium and tightened an overhand knot formed from 10-0 nylon suture around the primitive left atrium, decreasing its effective volume (Fig. 1) (Tobita et al., 2005). We repositioned the embryo to its original right-side up orientation, sealed the window with Parafilm (Pechiney Plastic Packaging, Menasha, WI), and reincubated for 1 hr to restore normal heart rhythms. Control embryos had only the overlying membrane removed and were injected immediately with no reincubation. Sham embryos had a slit made in the thoracic wall above the left atrium and were reincubated for one hour.

To inject embryos, we pulled needles from 1.0 mm inner diameter glass capillary pipettes to 15 μm inner diameter and a 30° bevel (PC-10 Puller, EG-44 Microgrinder, Narishige Inc., Japan). Needles were connected by means of polyethylene tubing (PE100, Braintree Scientific, Braintree, MA) to a 10 μl glass Hamilton gastight syringe (1701LT, Fisher Scientific, Waltham, MA). The syringe was mounted on a three-axis mechanical micromanipulator (Leica Microsystems GmbH, Germany). We primed the syringe, tubing, and needle with chick ringer's solution and then drew up 1 μl of Cy5-diethyl fluorescent dye diluted 1:1 in phosphate buffered saline (excitation wavelength 626 nm, emission wavelength 666 nm). Cy5 dyes were prepared at the Molecular Biosensor Imaging Center at CMU (Mujumdar et al., 1993). We injected embryos at three different venous sites: (1) RCCV, (2) RVV, and (3) LVV, with all embryos viewed in the right side up orientation (Fig. 1). Each embryo was placed under the stereomicroscope and the yolk sac membrane (RVV, LVV sites) or amnion (RCCV site) was removed above the injection site. The needle was inserted into the selected vein and a brightfield movie was recorded using a low light monochrome digital camera (Leica DFC 350FX, Leica Microsystems, GmbH, Germany). We then injected 0.3 μl of dye, visualized using an external fluorescent light source (Leica EL6000, Leica Microsystems, GmbH, Germany) and recorded the flow streams. This volume of injected dye has been shown to minimally affect normal hemodynamics, resulting in less than a 10% change in stroke volume and mean arterial pressure (Wagman et al., 1990). A total of 84 embryos were injected: 28 RCCV (12 control, 5 sham, 11 LAL), 29 RVV (17 control, 5 sham, 7 LAL), and 27 LVV (13 control, 6 sham, 8 LAL). Movies of each injection site for representative control and LAL embryos are provided in the . All injections were performed in ovo and only one site was injected per embryo.

Quantitative measurement of the intracardiac flow stream

We applied a quantitative approach to determine the location of the intracardiac streams. End-diastolic still images (696 × 520 pixels) were extracted from the recorded brightfield movies and used to manually identify the ventral and dorsal boundaries of the ventricle and outflow tract. The manually selected points were used to form polynomial expressions defining the shape of the ventral and dorsal margins, giving two continuous functions. We used the horizontal position as the independent variable, and rotated images, if necessary, so that the long axis of the heart was approximately horizontal. We then extracted still frames from the fluorescent recordings of the injections, which showed the flow stream as it passed through the ventricle and outflow tract. The centerline of the flow stream was manually identified and used to form a third polynomial expression. Any rotations applied to the brightfield image were applied exactly to the fluorescent image. For each point along the flow stream, we were then able to mathematically calculate the two points of intersection between the line normal to the stream and the ventral and dorsal walls of the heart. Using these intersection points, we then calculated the Euclidean distance between the centerline of the stream and the ventral (ε) and dorsal (δ) walls. The normalized intracardiac stream position was defined as $\delta/(\varepsilon+\delta)$. We computed the position for 10 evenly distributed points along the stream centerline and took the mean value as the final intracardiac stream position (Fig. 2). The entire process was performed using a semi-automated ad hoc program developed in MATLAB (R2011a, Mathworks, Natick, MA). We performed the analysis once per embryo.

The brightfield movie was recorded after insertion of the needle into the vessel, but before injection of the dye. The injection movie was then recorded without moving the embryo or changing the zoom level to facilitate direct overlapping. As a check, we can clearly observe that the dye within the needle seen in the fluorescent image directly overlaps with the bore of the needle visible in the brightfield image (Fig. 2). When performing our analysis, we rejected any overlays that did not meet this registration test. In addition, as the aortic arches, dorsal aorta, and extraembryonic vessels were filled with dye, their patterns directly overlapped with these vessels in the brightfield image, further demonstrating that no movement occurred between the recording of the brightfield and fluorescent data. When manually selecting the ventral and dorsal boundaries, we chose points along the outer surface of the heart, as it was easier to identify. Although these boundaries are not the inner lumen, we were consistent in our selection, allowing for a one to one comparison between control and LAL embryos.

We performed two-tailed, unpaired *t*-tests to determine differences in ICFP between groups. A *p*-value of less than 0.05 was considered significant.

Computational Fluid Dynamics Model of an *In Silico* LAL Stage 21 Heart

Creation of geometric heart loop models

We based the geometry and proportions of our control stage 21 heart loop model on a variety of anatomical imaging studies including serial histology (van den Berg and Moorman, 2011), scanning electron microscopy (Manner, 2000), micro computed tomography (Kim et al., 2011), magnetic resonance imaging (Yelbuz et al., 2003), and optical coherence tomography (Davis et al., 2008). The general "looped tube" structure was designed in Pro-Engineer (Parametric Technology Corp., Needham, MA) based on previous sketches and models (Patten, 1920; Manner, 2004). Atrial and ventricular bulbs, outflow tract tapering, and the venous inlets (RVV, LVV, and both CCV) were added using our in-house sketch-based anatomical editing tool, SketchCAD. The heart geometry was modeled at end diastole. The model was

completed and made CFD-ready using Geomagic Studio 10 (Geomagic Inc., Durham, NC). An in silico LAL surgery was performed by removing the presumptive left atrium volume and creating a smoothed surface to connect the left wall of the atrioventricular canal to the remaining right atrium, using our in-house surgical planning suite (Pekkan et al., 2008; Dur et al., 2011). The finished control and LAL models were rendered in Geomagic Studio 10 (Geomagic Inc., Durham, NC) and exported into GAMBIT (ANSYS Inc., Cannonsburg, PA), to create a surface triangular mesh. The triangular mesh was imported into our in-house CFD preprocessor, which generates an unstructured 3D Cartesian immersed boundary mesh. The immersed boundary grid had a spatial resolution of 14 μm for both the control and LAL models.

Computational fluid dynamics

Blood flow through the embryonic heart was modeled using our in-house immersed boundary cardiovascular flow solver incorporating a validated second-order accurate multi-grid artificial compressibility numerical method, described in our previous studies (Payli et al., 2007; Pekkan et al., 2009; Menon et al., 2012). Flow was simulated in terms of inlet normalized spatio-temporal units, on a high-resolution unstructured Cartesian immersed boundary grid with finite-difference numerical treatment. The objective of the CFD model was to determine if the geometric change of removing the left atrial volume was sufficient to alter ICFP and WSS. Therefore, we performed a steady-state simulation with fixed walls and no slip boundary conditions. The mean cardiac output of the stage 21 chick embryo, 1.28 mm^3/s (Yoshigi et al., 2000), was used to compute inflow boundary conditions at each of the four venous inlets. As reliable data for the venous flow rates was not available, we prescribed an inflow distribution of 25/75 between the blood returned from the embryo by the CCV and blood returned from the vitelline bed by the VV (Hu et al., 1996). Furthermore, a 50/50 split was specified between the cumulative inflows from the laterals. The Reynolds number (Re) of each of the CCV inlets was therefore 0.25, the Re of the VV inlets was 0.76, and the Re at the outflow tract was 2. A plug flow profile was assigned to all inlets. An instantaneous mass-flow preserving outflow boundary condition was adopted. Blood was treated as a Newtonian fluid with constant hemodynamic properties ($\rho = 1{,}060\ kg/m^3$, $\mu = 3.71 \times 10^{-3}$ Pa.s) (Al-Roubaie et al., 2011). In the case of the later stage model, which has only three inlets, the cardiac output remained the same, with 75% from the vitelline vein and 12.5% from each of the CCV. All other boundary conditions and assumptions were unchanged.

CFD simulations were conducted at Pittsburgh Supercomputing Center's Blacklight supercomputing cyber-infrastructure. Each simulation cost an average of 22 hr at 32 core parallelism. Convergence of the steady inflow CFD solution was monitored using the running average velocity field, which converged to steady state relatively quickly.

References

Al Naieb S, Happel CM, Yelbuz TM. 2013. A detailed atlas of chick heart development in vivo. Ann Anat 195:324–341.

Al-Roubaie S, Jahnsen ED, Mohammed M, Henderson-Toth C, Jones EA. 2011. Rheology of embryonic avian blood. Am J Physiol Heart Circ Physiol 301:H2473–H2481.

Atkins DL, Clark EB, Marvin WJ Jr. 1982. Foramen ovale/atrial septum area ratio: a marker of transatrial blood flow. Circulation 66: 281–283.

Bartman T, Walsh EC, Wen KK, McKane M, Ren J, Alexander J, Rubenstein PA, Stainier DY. 2004. Early myocardial function affects endocardial cushion development in zebrafish. PLoS Biol 2:E129.

Bayer IM, Adamson SL, Langille BL. 1999. Atrophic remodeling of the artery-cuffed artery. Arterioscler Thromb Vasc Biol 19:1499–1505.

Bremer JL. 1932. The presence and influence of two spiral streams in the heart of the chick embryo. Am J Anat 49:409–440.

Butcher JT, McQuinn TC, Sedmera D, Turner D, Markwald RR. 2007. Transitions in early embryonic atrioventricular valvular function correspond with changes in cushion biomechanics that are predictable by tissue composition. Circ Res 100: 1503–1511.

Chen CY, Menon PG, Kowalski WJ, Pekkan K. 2012. Time-resolved OCT-μPIV: a new μPIV technique applied to noninvasive and depth-resolved pulsatile flow measurements in microchannels and chick embryos. Exp Fluids 54:1496.

Chen CY, Patrick MJ, Corti P, Kowalski W, Roman BL, Pekkan K. 2011. Analysis of early embryonic great-vessel microcirculation in zebrafish using high-speed confocal μPIV. Biorheology 48:305–321.

Chin AJ, Weinberg PM, Barber G. 1990. Subcostal two-dimensional echocardiographic identification of anomalous attachment of septum primum in patients with left atrioventricular valve underdevelopment. J Am Coll Cardiol 15:678–681.

Clark EB, Hu N, Frommelt P, Vandekieft GK, Dummett JL, Tomanek RJ. 1989. Effect of increased pressure on ventricular growth in stage 21 chick embryos. Am J Physiol 257:H55–H61.

Corti P, Young S, Chen CY, Patrick MJ, Rochon ER, Pekkan K, Roman BL. 2011. Interaction between alk1 and blood flow in the development of arteriovenous malformations. Development 138: 1573–1582.

Culver JC, Dickinson ME. 2010. The effects of hemodynamic force on embryonic development. Microcirculation 17:164–178.

Davis AM, Rothenberg FG, Shepherd N, Izatt JA. 2008. In vivo spectral domain optical coherence tomography volumetric imaging and spectral Doppler velocimetry of early stage embryonic chicken heart development. J Opt Soc Am A Opt Image Sci Vis 25:3134–3143.

De la Cruz MV, Gimenez-Ribotta M, Saravalli O, Cayre R. 1983. The contribution of the inferior endocardial cushion of the atrioventricular canal to cardiac septation and to the development of the atrioventricular valves: study in the chick embryo. Am J Anat 166:63–72.

de la Pompa JL, Timmerman LA, Takimoto H, Yoshida H, Elia AJ, Samper E, Potter J, Wakeham A, Marengere L, Langille BL, Crabtree GR, Mak TW. 1998. Role of the NF-ATc transcription factor in morphogenesis of cardiac valves and septum. Nature 392:182–186.

deAlmeida A, McQuinn T, Sedmera D. 2007. Increased ventricular preload is compensated by myocyte proliferation in normal and hypoplastic fetal chick left ventricle. Circ Res 100: 1363–1370.

DeGroff CG, Thornburg BL, Pentecost JO, Thornburg KL, Gharib M, Sahn DJ, Baptista A. 2003. Flow in the early embryonic human heart: a numerical study. Pediatr Cardiol 24:375–380.

Dunker N, Krieglstein K. 2002. Tgfbeta2 -/- Tgfbeta3 -/- double knockout mice display severe midline fusion defects and early embryonic lethality. Anat Embryol (Berl) 206:73–83.

Dur O, Coskun ST, Coskun KO, Frakes D, Kara LB, Pekkan K. 2011. Computer-aided Patient-specific coronary artery graft design improvements using CFD coupled shape optimizer. Cardiovasc Eng Technol 2:35–47.

Egorova AD, Van der Heiden K, Van de Pas S, Vennemann P, Poelma C, DeRuiter MC, Goumans MJ, Gittenberger-de Groot AC, ten Dijke P, Poelmann RE, Hierck BP. 2011. Tgfbeta/Alk5 signaling is required for shear stress induced klf2 expression in embryonic endothelial cells. Dev Dyn 240:1670–1680.

Feinstein JA, Benson DW, Dubin AM, Cohen MS, Maxey DM, Mahle WT, Pahl E, Villafane J, Bhatt AB, Peng LF, Johnson BA, Marsden AL, Daniels CJ, Rudd NA, Caldarone CA, Mussatto KA, Morales DL, Ivy DD, Gaynor JW, Tweddell JS, Deal BJ, Furck AK, Rosenthal GL, Ohye RG, Ghanayem NS, Cheatham JP, Tworetzky W, Martin GR. 2012. Hypoplastic left heart syndrome:

current considerations and expectations. J Am Coll Cardiol 59: S1–S42.
Feit LR, Copel JA, Kleinman CS. 1991. Foramen ovale size in the normal and abnormal human fetal heart: an indicator of transatrial flow physiology. Ultrasound Obstet Gynecol 1:313–319.
Franz T. 1989. Persistent truncus arteriosus in the Splotch mutant mouse. Anat Embryol (Berl) 180:457–464.
Friedman S, Murphy L, Ash R. 1951. Aortic atresia with hypoplasia of the left heart and aortic arch. J Pediatr 38:354–368.
Gessner IH. 1966. Spectrum of congenital cardiac anomalies produced in chick embryos by mechanical interference with cardiogenesis. Circ Res 18:625–633.
Girerd X, London G, Boutouyrie P, Mourad JJ, Safar M, Laurent S. 1996. Remodeling of the radial artery in response to a chronic increase in shear stress. Hypertension 27:799–803.
Go AS, Mozaffarian D, Roger VL, Benjamin EJ, Berry JD, Borden WB, Bravata DM, Dai S, Ford ES, Fox CS, Franco S, Fullerton HJ, Gillespie C, Hailpern SM, Heit JA, Howard VJ, Huffman MD, Kissela BM, Kittner SJ, Lackland DT, Lichtman JH, Lisabeth LD, Magid D, Marcus GM, Marelli A, Matchar DB, McGuire DK, Mohler ER, Moy CS, Mussolino ME, Nichol G, Paynter NP, Schreiner PJ, Sorlie PD, Stein J, Turan TN, Virani SS, Wong ND, Woo D, Turner MB. 2013. Heart disease and stroke statistics–2013 update: a report from the American Heart Association. Circulation 127:e6–e245.
Groenendijk BC, Hierck BP, Vrolijk J, Baiker M, Pourquie MJ, Gittenberger-de Groot AC, Poelmann RE. 2005. Changes in shear stress-related gene expression after experimentally altered venous return in the chicken embryo. Circ Res 96:1291–1298.
Grossfeld P, Ye M, Harvey R. 2009. Hypoplastic left heart syndrome: new genetic insights. J Am Coll Cardiol 53:1072–1074.
Hamburger V, Hamilton HL. 1951. A series of normal stages in the development of the chick embryo. J Morphol 88:49–92.
Hinton RB Jr, Martin LJ, Tabangin ME, Mazwi ML, Cripe LH, Benson DW. 2007. Hypoplastic left heart syndrome is heritable. J Am Coll Cardiol 50:1590–1595.
Hinton RB, Martin LJ, Rame-Gowda S, Tabangin ME, Cripe LH, Benson DW. 2009. Hypoplastic left heart syndrome links to chromosomes 10q and 6q and is genetically related to bicuspid aortic valve. J Am Coll Cardiol 53:1065–1071.
Hogers B, DeRuiter MC, Baasten AM, Gittenberger-de Groot AC, Poelmann RE. 1995. Intracardiac blood flow patterns related to the yolk sac circulation of the chick embryo. Circ Res 76:871–877.
Hogers B, DeRuiter MC, Gittenberger-de Groot AC, Poelmann RE. 1997. Unilateral vitelline vein ligation alters intracardiac blood flow patterns and morphogenesis in the chick embryo. Circ Res 80:473–481.
Hogers B, DeRuiter MC, Gittenberger-de Groot AC, Poelmann RE. 1999. Extraembryonic venous obstructions lead to cardiovascular malformations and can be embryolethal. Cardiovasc Res 41: 87–99.
Hove JR, Koster RW, Forouhar AS, Acevedo-Bolton G, Fraser SE, Gharib M. 2003. Intracardiac fluid forces are an essential epigenetic factor for embryonic cardiogenesis. Nature 421:172–177.
Hu N, Christensen DA, Agrawal AK, Beaumont C, Clark EB, Hawkins JA. 2009. Dependence of aortic arch morphogenesis on intracardiac blood flow in the left atrial ligated chick embryo. Anat Rec (Hoboken) 292:652–660.
Hu N, Clark EB. 1989. Hemodynamics of the stage 12 to stage 29 chick embryo. Circ Res 65:1665–1670.
Hu N, Ngo TD, Clark EB. 1996. Distribution of blood flow between embryo and vitelline bed in the stage 18, 21 and 24 chick embryo. Cardiovasc Res 31 Spec No:E127–E131.
Hurlstone AF, Haramis AP, Wienholds E, Begthel H, Korving J, Van Eeden F, Cuppen E, Zivkovic D, Plasterk RH, Clevers H. 2003. The Wnt/beta-catenin pathway regulates cardiac valve formation. Nature 425:633–637.
Jaffee OC. 1965. Hemodynamic factors in the development of the chick embryo heart. Anat Rec 151:69–75.
Jaffee OC. 1967. The development of the arterial outflow tract in the chick embryo heart. Anat Rec 158:35–42.
Kim JS, Min J, Recknagel AK, Riccio M, Butcher JT. 2011. Quantitative three-dimensional analysis of embryonic chick morphogenesis via microcomputed tomography. Anat Rec (Hoboken) 294: 1–10.
Kowalski WJ, Dur O, Wang Y, Patrick MJ, Tinney JP, Keller BB, Pekkan K. 2013. Critical transitions in early embryonic aortic arch patterning and hemodynamics. PLoS One 8:e60271.
Langille BL, O'Donnell F. 1986. Reductions in arterial diameter produced by chronic decreases in blood flow are endothelium-dependent. Science 231:405–407.
Liu A, Nickerson A, Troyer A, Yin X, Cary R, Thornburg K, Wang R, Rugonyi S. 2011. Quantifying blood flow and wall shear stresses in the outflow tract of chick embryonic hearts. Comput Struct 89:855–867.
Lucitti JL, Tobita K, Keller BB. 2005. Arterial hemodynamics and mechanical properties after circulatory intervention in the chick embryo. J Exp Biol 208:1877–1885.
Lucitti JL, Visconti R, Novak J, Keller BB. 2006. Increased arterial load alters aortic structural and functional properties during embryogenesis. Am J Physiol Heart Circ Physiol 291:H1919–H1926.
Manner J. 2000. Cardiac looping in the chick embryo: a morphological review with special reference to terminological and biomechanical aspects of the looping process. Anat Rec 259:248–262.
Manner J. 2004. On rotation, torsion, lateralization, and handedness of the embryonic heart loop: new insights from a simulation model for the heart loop of chick embryos. Anat Rec A Discov Mol Cell Evol Biol 278:481–492.
Manner J, Merkel N. 2007. Early morphogenesis of the sinuatrial region of the chick heart: a contribution to the understanding of the pathogenesis of direct pulmonary venous connections to the right atrium and atrial septal defects in hearts with right isomerism of the atrial appendages. Anat Rec (Hoboken) 290:168–180.
Martinsen BJ. 2005. Reference guide to the stages of chick heart embryology. Dev Dyn 233:1217–1237.
McBride KL, Zender GA, Fitzgerald-Butt SM, Koehler D, Menesses-Diaz A, Fernbach S, Lee K, Towbin JA, Leal S, Belmont JW. 2009. Linkage analysis of left ventricular outflow tract malformations (aortic valve stenosis, coarctation of the aorta, and hypoplastic left heart syndrome). Eur J Hum Genet 17:811–819.
McElhinney DB, Tworetzky W, Lock JE. 2010. Current status of fetal cardiac intervention. Circulation 121:1256–1263.
Menon PG, Sotiropoulos F, Pekkan K. 2012. CFD challenge: computational hemodynamics analysis of patient-specific internal carotid artery aneursym using an in-house finite difference cardiovascular flow solver. In: ASME Summer Bioengineering Conference. Fajardo, Puerto Rico.
Mujumdar RB, Ernst LA, Mujumdar SR, Lewis CJ, Waggoner AS. 1993. Cyanine dye labeling reagents: sulfoindocyanine succinimidyl esters. Bioconjug Chem 4:105–111.
Myers CD, Mattix K, Presson RG Jr, Vijay P, Maynes D, Litwak KN, Brown JW, Rodefeld MD. 2006. Twenty-four hour cardiopulmonary stability in a model of assisted newborn Fontan circulation. Ann Thorac Surg 81:264–270; discussion 270–271.
Noden DM. 1991. Origins and patterning of avian outflow tract endocardium. Development 111:867–876.
Noonan JA, Nadas AS. 1958. The hypoplastic left heart syndrome; an analysis of 101 cases. Pediatr Clin North Am 5:1029–1056.
Patten BM. 1920. The early embryology of the chick. Philadelphia: P. Blakiston's Son and Co. 167 p.
Payli R, Pekkan K, Zelicourt D, Frakes D, Sotiropoulos F, Yoganathan A. 2007. High performance clinical computing on the TeraGrid: patient-specific hemodynamic analysis and surgical planning. In: TeraGrid 2007 Conference Madison, WI.
Pekkan K, Dur O, Zelicourt D, Payli R, Sotiropoulos F, Kowalski WJ, Chen C-Y, Patrick MJ, Kara L, Keller BB. 2009. Embryonic intra-cardiac flow fields at three idealized ventricular morphologies. In: 62nd Annual Meeting of the APS Division of Fluid Dynamics. Minneapolis, MN.
Pekkan K, Keller BB. 2013. Guest editorial: special issue on fetal hemodynamics. Cardiovasc Eng Technol:1–3.
Pekkan K, Whited B, Kanter K, Sharma S, de Zelicourt D, Sundareswaran K, Frakes D, Rossignac J, Yoganathan AP. 2008. Patient-specific surgical planning and hemodynamic computational

fluid dynamics optimization through free-form haptic anatomy editing tool (SURGEM). Med Biol Eng Comput 46:1139–1152.
Pexieder T. 1986. Standardized method for study of normal and abnormal cardiac development in chick, rat, mouse, dog and human embryos. Teratology 33:91C–92C.
Poelma C, Van der Heiden K, Hierck BP, Poelmann RE, Westerweel J. 2010. Measurements of the wall shear stress distribution in the outflow tract of an embryonic chicken heart. J R Soc Interface 7:91–103.
Qayyum SR, Webb S, Anderson RH, Verbeek FJ, Brown NA, Richardson MK. 2001. Septation and valvar formation in the outflow tract of the embryonic chick heart. Anat Rec 264:273–283.
Ranger AM, Grusby MJ, Hodge MR, Gravallese EM, de la Brousse FC, Hoey T, Mickanin C, Baldwin HS, Glimcher LH. 1998. The transcription factor NF-ATc is essential for cardiac valve formation. Nature 392:186–190.
Reckova M, Rosengarten C, deAlmeida A, Stanley CP, Wessels A, Gourdie RG, Thompson RP, Sedmera D. 2003. Hemodynamics is a key epigenetic factor in development of the cardiac conduction system. Circ Res 93:77–85.
Rodbard S. 1975. Vascular caliber. Cardiology 60:4–49.
Rodefeld MD, Boyd JH, Myers CD, LaLone BJ, Bezruczko AJ, Potter AW, Brown JW. 2003. Cavopulmonary assist: circulatory support for the univentricular Fontan circulation. Ann Thorac Surg 76:1911–1916.
Rychik J, Rome JJ, Collins MH, DeCampli WM, Spray TL. 1999. The hypoplastic left heart syndrome with intact atrial septum: atrial morphology, pulmonary vascular histopathology and outcome. J Am Coll Cardiol 34:554–560.
Rychter Z. 1962. Experimental morphology of the aortic arches and the heart loop in chick embryos. Adv Morphog 2:333–371.
Rychter Z, Lemez L. 1958. Acta Universitatis Carolinae: Medica. Supplementum 5:299–309.
Rychter Z, Lemez L. 1965. Changes in localization in aortic arches of laminar blood streams of main venous trunks to heart after exclusion of vitelline vessels on second day of incubation. Fed Proc Transl Suppl 24:815–820.
Schroder EA, Tobita K, Tinney JP, Foldes JK, Keller BB. 2002. Microtubule involvement in the adaptation to altered mechanical load in developing chick myocardium. Circ Res 91:353–359.
Sedmera D, Cook AC, Shirali G, McQuinn TC. 2005. Current issues and perspectives in hypoplasia of the left heart. Cardiol Young 15:56–72.
Sedmera D, Hu N, Weiss KM, Keller BB, Denslow S, Thompson RP. 2002. Cellular changes in experimental left heart hypoplasia. Anat Rec 267:137–145.
Sedmera D, Pexieder T, Rychterova V, Hu N, Clark EB. 1999. Remodeling of chick embryonic ventricular myoarchitecture under experimentally changed loading conditions. Anat Rec 254: 238–252.
Sedmera D, Pexieder T, Vuillemin M, Thompson RP, Anderson RH. 2000. Developmental patterning of the myocardium. Anat Rec 258:319–337.
Tallquist MD, Soriano P. 2003. Cell autonomous requirement for PDGFRalpha in populations of cranial and cardiac neural crest cells. Development 130:507–518.
Tobita K, Garrison JB, Liu LJ, Tinney JP, Keller BB. 2005. Three-dimensional myofiber architecture of the embryonic left ventricle during normal development and altered mechanical loads. Anat Rec A Discov Mol Cell Evol Biol 283:193–201.
Tobita K, Keller BB. 2000. Right and left ventricular wall deformation patterns in normal and left heart hypoplasia chick embryos. Am J Physiol Heart Circ Physiol 279:H959–H969.
van den Berg G, Moorman AF. 2011. Development of the pulmonary vein and the systemic venous sinus: an interactive 3D overview. PLoS One 6:e22055.
Wagman AJ, Hu N, Clark EB. 1990. Effect of changes in circulating blood-volume on cardiac-output and arterial and ventricular blood-pressure in the stage-18, stage-24, and stage-29 chick-embryo. Circ Res 67:187–192.
Wang Y, Dur O, Patrick MJ, Tinney JP, Tobita K, Keller BB, Pekkan K. 2009. Aortic arch morphogenesis and flow modeling in the chick embryo. Ann Biomed Eng 37:1069–1081.
Yalcin HC, Shekhar A, McQuinn TC, Butcher JT. 2011. Hemodynamic patterning of the avian atrioventricular valve. Dev Dyn 240:23–35.
Yelbuz TM, Zhang X, Choma MA, Stadt HA, Zdanowicz M, Johnson GA, Kirby ML. 2003. Images in cardiovascular medicine. Approaching cardiac development in three dimensions by magnetic resonance microscopy. Circulation 108:e154–e155.
Yoshida H, Manasek F, Arcilla RA. 1983. Intracardiac flow patterns in early embryonic life. A reexamination. Circ Res 53: 363–371.
Yoshigi M, Knott GD, Keller BB. 2000. Lumped parameter estimation for the embryonic chick vascular system: a time-domain approach using MLAB. Comput Methods Programs Biomed 63: 29–41.